Optics Letters

Simultaneous generation of sub-5-femtosecond 400 nm and 800 nm pulses for attosecond extreme ultraviolet pump–probe spectroscopy

Hung-Tzu Chang,[1,6,†] Michael Zürch,[1,4,†] Peter M. Kraus,[1] Lauren J. Borja,[1] Daniel M. Neumark,[1,2,5] and Stephen R. Leone[1,2,3,*]

[1]Department of Chemistry, University of California, Berkeley, California 94720, USA
[2]Chemical Sciences Division, Lawrence Berkeley National Laboratory, Berkeley, California 94720, USA
[3]Department of Physics, University of California, Berkeley, California 94720, USA
[4]e-mail: mwz@berkeley.edu
[5]e-mail: dneumark@berkeley.edu
[6]e-mail: htchang@berkeley.edu
*Corresponding author: srl@berkeley.edu

Received 15 August 2016; accepted 18 October 2016; posted 25 October 2016 (Doc. ID 273714); published 15 November 2016

Few-cycle laser pulses with wavelengths centered at 400 nm and 800 nm are simultaneously obtained through wavelength separation of ultrashort, spectrally broadened Vis–NIR laser pulses spanning 350–1100 nm wavelengths. The 400 nm and 800 nm pulses are separately compressed, yielding pulses with 4.4 fs and 3.8 fs duration, respectively. The pulse energy exceeds 5 μJ for the 400 nm pulses and 750 μJ for the 800 nm pulses. Intense 400 nm few-cycle pulses have a broad range of applications in nonlinear optical spectroscopy, which include the study of photochemical dynamics, semiconductors, and photovoltaic materials on few-femtosecond to attosecond time scales. The ultrashort 400 nm few-cycle pulses generated here not only extend the spectral range of the optical pulse for NIR–XUV attosecond pump–probe spectroscopy but also pave the way for two-color, three-pulse, multidimensional optical–XUV spectroscopy experiments.

OCIS codes: (320.7150) Ultrafast spectroscopy; (320.5520) Pulse compression; (320.7110) Ultrafast nonlinear optics.

http://dx.doi.org/10.1364/OL.41.005365

Ultrashort few-cycle optical pulses are indispensable for attosecond optical spectroscopy, which is used to investigate electron dynamics in atoms, molecules, and solids [1–8]. In a typical NIR–XUV attosecond pump–probe experiment, a compressed intense NIR pulse is split off and focused onto a noble gas to generate an XUV pulse through high-harmonic generation (HHG), while the remainder forms a NIR pump pulse. Attosecond NIR–XUV pump–probe spectroscopy is highly useful in investigating charge-carrier dynamics and strong-field phenomena in semiconductors [6–13]. However, to investigate attosecond charge-carrier dynamics in wide-bandgap (>2.5 eV) semiconductors through one-photon excitation, it is valuable to develop a scheme to generate sub-5-fs 400 nm optical pulses at energies sufficient to perform pump–probe measurements in addition to the strong few-cycle pulse that is used to generate the attosecond probe pulse. Moreover, intense few-cycle 400 nm pulses will provide few-femtosecond or even subfemtosecond time-resolution in many UV–Vis nonlinear optical spectroscopies in the 350–500 nm region. Simultaneous generation of few-cycle 400 nm and 800 nm pulses further enables optical excitation within the whole visible range, which is extremely useful for studying excited-state dynamics in photovoltaic materials and photosynthetic light-harvesting systems [14,15].

Generation of 400 nm laser pulses can be achieved by frequency upconversion of an 800 nm Ti:sapphire laser pulse. However, directly generating sub-5-fs 400 nm pulses through frequency doubling of compressed 800 nm pulses requires extremely thin nonlinear crystals. For example, obtaining a 5 fs transform-limited 400 nm pulse in a BBO crystal requires <30 μm substrate thickness [16], which subsequently limits the output energy of the 400 nm pulse. Sub-10-fs 400 nm pulses with sufficient energy for pump–probe experiments have been reported using thick (>100 μm) BBO crystals. There, sufficient spectral bandwidth is obtained via broadband frequency doubling [17–20], where the incoming beam is angularly dispersed and recollimated by a pair of gratings to achieve the desired phase-matching angle for different input wavelengths or self-phase modulation in a hollow-core fiber with subsequent dispersion compensation [21–24]. Varillas *et al.* obtained 8 fs 400 nm pulses with ∼40 nm spectral width using broadband sum-frequency generation [20]. With noncollinear broadband sum-frequency generation, Grün *et al.* successfully generated compressed, 400 nm pulses with pulse duration of 32 fs and pulse energy of 55 μJ using 800 nm pulses with 74 fs pulse duration [25]. Employing an Ar-filled hollow-core fiber, Kobayashi and co-workers successfully broadened and compressed 400 nm laser pulses from second-harmonic

generation in a BBO crystal with 80 nm spectral width and 7.5 fs pulse duration [24]. However, compression of 400 nm pulses to below 5 fs duration requires even greater spectral bandwidth (>100 nm) in the output pulse. In broadband frequency doubling, this would require a broader spectral range of the input pulse and wider angular dispersion to achieve phase matching of all input wavelengths or a much thinner nonlinear medium. These constraints either pose challenges in compensating the high-order angular dispersion or preclude efficient energy conversion. The compression of pulses using a hollow-core fiber will require shorter input pulses to avoid fragmentation of the output pulses in the time domain, while the duration of the input pulse is restricted by the phase-matching bandwidth of the BBO crystal and the pulse duration from the Ti:sapphire amplifier [24].

In pioneering work, Nisoli *et al.* showed that high-energy (>500 μJ) laser pulses can be spectrally broadened in a gas-filled hollow-core fiber to obtain pulses with 10 fs duration [26]. Goulielmakis and co-workers demonstrated that direct spectral broadening of an 800 nm laser pulse in a Ne-filled hollow-core fiber can yield pulses with an ultrabroadband spectrum ranging from 300 to 1100 nm [27–29]. Subsequent dichroic splitting of the supercontinuum into various spectral components from the ultrabroadband pulse yields 6–9 fs pulses across four separate wavelength components, which are successively recombined to generate optical attosecond pulses [29]. With 1 mJ, ~22 fs, 800 nm input pulses, the resulting pulse energy of the four wavelength components can reach ~320 μJ in total [29].

Here we report on the generation of 400 nm laser pulses with up to 5 μJ pulse energy with sub-5-fs pulse duration through dichroic beam splitting of a portion of the spectrally broadened pulse from a hollow-core fiber, while the spectrum and pulse energy around 800 nm necessary for attosecond XUV generation is fully preserved (>750 μJ). We also demonstrate long-term energy stability of the two pulses, making this pulse pair well-suited for ultrafast optical–XUV pump–probe experiments.

To generate ultrabroadband pulses spanning the 350–1100 nm spectral range, 1.5 mJ pulses with approximately 27 fs duration at 1 kHz repetition rate produced from a chirped pulse amplification (CPA) Ti:sapphire amplifier (Femtolasers FemtoPower Compact PRO) are focused into a 1 m long, 320 μm diameter hollow-core fiber filled with 2–2.8 bar Ne (Fig. 1). A typical spectrum and autocorrelation trace of the pulse from the amplifier are shown in Figs. 1(b) and 1(c), respectively. The beam is spectrally broadened in the hollow-core fiber and subsequently separated by a 1 mm thick dichroic beam splitter, with the front surface coated to reflect 350–500 nm and the rear surface antireflection coated for 520 to 940 nm. The layers are optimized for low group-delay dispersion (Layertec GmbH). In two separate arms, the transmitted and reflected beams are recollimated and separately compressed by two different sets of double-angle chirped mirrors (Ultrafast Innovations GmBH) and two pairs of fused silica wedges for fine dispersion compensation (Fig. 1). Because the 800 nm double-angle chirped mirrors for the transmitted beam only support wavelengths ranging from 500 to 1050 nm, separating the light with wavelengths below 500 nm compromises neither the energy nor the spectral bandwidth of 800 nm pulses.

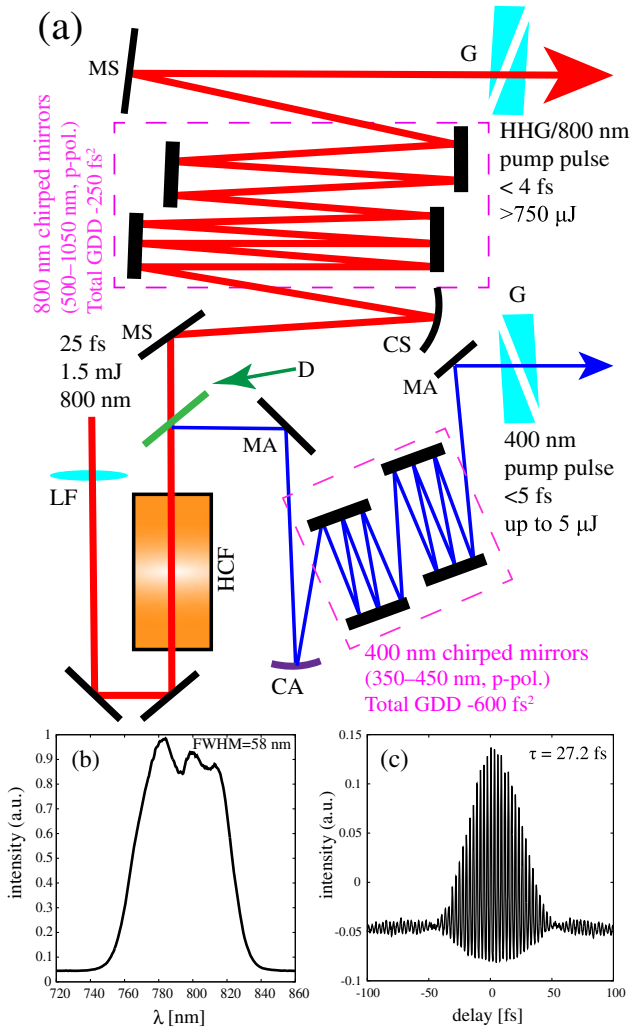

Fig. 1. Experimental setup and the characterization of the input pulse. (a) The experimental setup for broadening, separation, and compression of the pulses. HCF, 1 m Ne-filled hollow-core fiber; D, 1 mm thick dichroic beam splitter; G, fused silica wedges; LF, convex lens ($f = 2$ m); CS, concave silver-coated mirror ($f = 1500$ mm); CA, concave aluminum-coated mirror ($f = 750$ mm); MA, planar aluminum-coated mirror; MS, planar silver-coated mirror. (b) Spectrum and (c) autocorrelation trace of the input pulse from the Ti:sapphire amplifier.

Spectra of the transmitted and reflected beams are shown in Fig. 2(a). The spectrum of the 400 nm pulses spans 350 to 500 nm, featuring ~150 nm bandwidth supporting <4 fs transform-limited pulses. Additionally, the 800 nm transmitted beam exhibits spectral bandwidth spanning 500–950 nm, which sets a transform limit of 3.2 fs to the pulse duration. By optimizing the Ne pressure in the hollow-core fiber, 400 nm and 800 nm pulses with pulse energies more than 5 μJ and 750 μJ, respectively, are readily obtainable. Figure 2(b) displays the evolution of pulse energy of both beams over 12 h. With 2.8 bar Ne in the hollow-core fiber, the 400 nm beam yields >5 μJ pulse energy with ~6% variance, while the 800 nm beam provides 780–800 μJ pulse energy with <0.5% variance. The strong dependence of the spectral broadening in the hollow-core fiber can also be

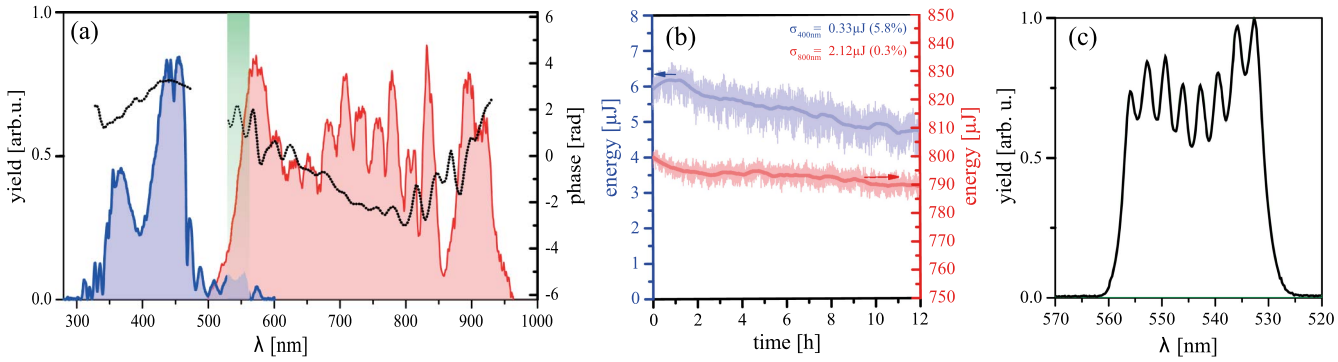

Fig. 2. Properties of 800 nm and 400 nm pulses after compression. (a) Spectra of 400 nm (blue) and 800 nm (red) pulses and their retrieved spectral phase (dotted line). The green shade indicates the overlapping spectral region of the compressed 400 nm and 800 nm pulses. (b) Long-time stability of 400 nm (blue) and 800 nm (red) pulse energy over 12 h with 2.8 bar Ne in the hollow-core fiber. (c) Measured spectra when the 400 nm and 800 nm pulses are overlapped in time with a 525–560 nm bandpass filter.

observed in the long-time decrease in pulse energy. Over 12 h, the pulse energy of the 400 nm beam decreases from ~6 μJ to ~5 μJ (<17%) due to leakage of high-pressure Ne from the hollow-core fiber chamber, while the energy of the 800 nm pulses decreases by less than 20 μJ (<3%).

The temporal structures of the 400 nm and 800 nm pulses are characterized by self-diffraction frequency-resolved optical gating (SD-FROG) [30,31] and dispersion scan (D-Scan, Sphere Ultrafast Photonics) [32], respectively. The self-diffraction signal is obtained by wavefront splitting of the 400 nm beam using two D-shaped mirrors on delay-scanning stages and subsequently focusing the two beams into a 100 μm thick sapphire crystal with a crossing angle of 50 mrad. Typical D-Scan and SD-FROG traces are shown in Figs. 3(a) and 3(b), respectively. The intensity profile [Fig. 3(c), blue line] and spectral phase [Fig. 2(a)] of the 400 nm pulse is retrieved using commercial software [33], yielding pulses with 4.4 ± 0.5 fs duration. On the other hand, the retrieval from the dispersion scan measurement shows that the pulse duration of the 800 nm beam is 3.8 ± 0.2 fs [Fig. 3(c), red line]. The measurements clearly show that sub-5-fs pulses at the central wavelength for both 400 nm and 800 nm can be simultaneously obtained through spectral broadening of the output of a standard Ti:sapphire amplifier in a hollow-core fiber and subsequent wavelength separation.

In a pump–probe experiment, the pump and probe pulses must overlap in both space and time. Within the presented setup, we demonstrate that the overlap of two pulses in time can be directly performed by observing the spectral interference of the two pulses in the 525–560 nm spectral region. Figure 2(a) shows that the 400 nm and 800 nm pulses share a common spectral region between 500 nm and 600 nm. Focusing the two beams into a spectrometer (HR4000, Ocean Optics) and with a bandpass filter (525–560 nm) to block the nonoverlapping spectral region, clear spectral interference between the two beams is observed [Fig. 2(c)]. The interferometric stability of the pump and probe arm can be inferred from the stability of the interferogram [Fig. 2(c)]. However, the interferometric stability highly depends on the path length and optical elements between compression and recollimation. Here we only show the interferogram that is used to find the time overlap of the 400 nm and 800 nm beam, and no estimate of the jitter between the 400 nm and 800 nm beam was made. The ease of determining the time overlap in this experimental setup makes it feasible for pump–probe and multidimensional spectroscopic experiments.

In summary, we demonstrate simultaneous generation of sub-5-fs pulses in both the 800 nm and 400 nm spectral region through wavelength separation of a supercontinuum produced in a Ne-filled hollow-core fiber. To the best of our knowledge, the reported pulse duration of 4.4 fs, comprising only three

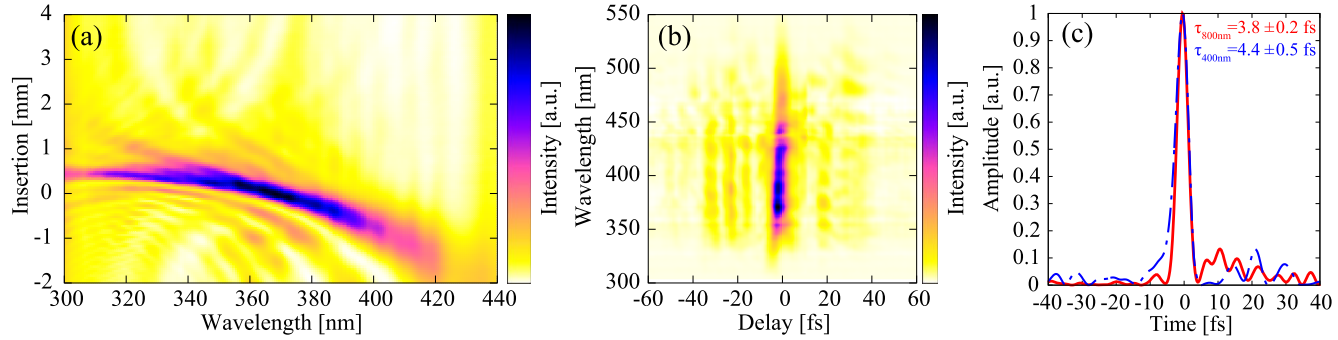

Fig. 3. Temporal profiles of 800 nm and 400 nm pulses after compression. (a) The measured dispersion scan trace of the 800 nm pulse. (b) The measured two-dimensional SD-FROG trace of the 400 nm pulses. (c) The retrieved temporal profile of the 400 nm (blue, dashed–dotted) and 800 nm (red) pulses. The hollow-core fiber is filled with 2.2 bar Ne. The pulse energy of the 400 nm and 800 nm beam are 1.6 and 800 μJ, respectively.

optical cycles, is the shortest value achieved thus far for blue light pulses. The intensity of the 400 nm pulses strongly depends on the self-phase modulation determined by the Ne pressure in the hollow-core fiber and thus it is possible to tune the energy of the 400 nm pulse by changing the pressure in the hollow-core fiber. Up to 5 μJ pulse energy in 400 nm pulses can be obtained by focusing the 1.5 mJ, 27 fs laser pulses into the hollow-core fiber while maintaining more than 750 μJ pulse energy around 800 nm for generating attosecond pulses via HHG. It is worth noting that although changing the gas pressure affects the spectrum of the 400 nm pulses, it is possible to adjust the energy from 1 to 5 μJ while maintaining sub-5-fs pulse duration. This setup enables direct optical excitation across the whole visible range with sub-5-fs time resolution for pump–probe and multidimensional spectroscopic experiments. Focusing the 400 nm beam to 10 μm focal diameter will result in an intensity of $\sim 10^{14}$ W/cm^2, which is sufficient for studying strong-field phenomena. Furthermore, nonlinear crystals are absent in this setup and thus it is not prone to optical damage. This method provides further energy scalability by increasing the energy of the input pulse. The use of a gas-filled hollow-core fiber as the broadening medium also allows changing the energy ratio between the blue and the red portion by altering the input wavelength. Our setup extends the spectral region of the optical pump in attosecond pump–probe experiments down to 350 nm. The demonstrated approach can be easily implemented in any regular few-cycle compression setup and opens up new experimental possibilities. In existing NIR–XUV pump–probe setups, an additional pump channel can be created without compromising the capabilities of the original beamline, and this further paves the way for multidimensional UV–Vis–XUV spectroscopy on the attosecond time scale.

Funding. Alexander von Humboldt-Stiftung; Army Research Office (ARO) (WN911NF-14-1-0383); Schweizerische Nationalfonds zur Förderung der Wissenschaftlichen Forschung (SNSF) (P2EZP2_165252); Air Force Office of Scientific Research (AFOSR) (FA9550-15-1-0037).

Acknowledgment. M. Z. acknowledges support from the Humboldt Foundation, and the experimental work is supported by ARO. P. M. K. acknowledges support from the SNSF. H.-T. C. and L. J. B. acknowledge support by AFOSR.

[†]These authors contributed equally to this work.

REFERENCES

1. M. Hentschel, R. Kienberger, C. Spielmann, G. A. Reider, N. Milosevic, T. Brabec, P. Corkum, U. Heinzmann, M. Drescher, and F. Krausz, Nature **414**, 509 (2001).
2. F. Krausz and M. Ivanov, Rev. Mod. Phys. **81**, 163 (2009).
3. M. F. Kling and M. J. J. Vrakking, Annu. Rev. Phys. Chem. **59**, 463 (2008).
4. L. Gallmann, C. Cirelli, and U. Keller, Annu. Rev. Phys. Chem. **63**, 447 (2012).
5. F. Krausz and M. I. Stockman, Nat. Photonics **8**, 205 (2014).
6. Z. Chang, P. B. Corkum, and S. R. Leone, J. Opt. Soc. Am. B **33**, 1081 (2016).
7. L. J. Borja, M. Zürch, C. D. Pemmaraju, M. Schultze, K. Ramasesha, A. Gandman, J. S. Prell, D. Prendergast, D. M. Neumark, and S. R. Leone, J. Opt. Soc. Am. B **33**, C57 (2016).
8. K. Ramasesha, S. R. Leone, and D. M. Neumark, Annu. Rev. Phys. Chem. **67**, 41 (2016).
9. M. Schultze, E. M. Bothschafter, A. Sommer, S. Holzner, W. Schweinberger, M. Fiess, M. Hofstetter, R. Kienberger, V. Apalkov, V. S. Yakovlev, M. I. Stockman, and F. Krausz, Nature **493**, 75 (2012).
10. M. Schultze, K. Ramasesha, C. D. Pemmaraju, S. A. Sato, D. Whitmore, A. Gandman, J. S. Prell, L. J. Borja, D. Prendergast, K. Yabana, D. M. Neumark, and S. R. Leone, Science **346**, 1348 (2014).
11. T. T. Luu, M. Garg, S. Y. Kruchinin, A. Moulet, M. T. Hassan, and E. Goulielmakis, Nature **521**, 498 (2015).
12. W. A. Okell, T. Witting, D. Fabris, C. A. Arrell, J. Hengster, S. Ibrahimkutty, A. Seiler, M. Barthelmess, S. Stankov, D. Y. Lei, Y. Sonnefraud, M. Rahmani, T. Uphues, S. A. Maier, J. P. Marangos, and J. W. G. Tisch, Optica **2**, 383 (2015).
13. H. Mashiko, K. Oguri, T. Yamaguchi, A. Suda, and H. Gotoh, Nat. Phys. **12**, 741 (2016).
14. C. Brabec, V. Dyakonov, J. Parisi, and N. Sariciftci, *Organic Photovoltaics: Concepts and Realization, Springer Series in Materials Science* (Springer, 2003).
15. R. Blankenship, *Molecular Mechanisms of Photosynthesis* (Wiley, 2002).
16. W. J. Alford and A. V. Smith, J. Opt. Soc. Am. B **18**, 515 (2001).
17. T. Kanai, X. Zhou, T. Sekikawa, S. Watanabe, and T. Togashi, Opt. Lett. **28**, 1484 (2003).
18. T. Kanai, X. Zhou, T. Liu, A. Kosuge, T. Sekikawa, and S. Watanabe, Opt. Lett. **29**, 2929 (2004).
19. X. Zhou, T. Kanai, D. Yoshitomi, T. Sekikawa, and S. Watanabe, Appl. Phys. B **81**, 13 (2005).
20. R. B. Varillas, A. Candeo, D. Viola, M. Garavelli, S. De Silvestri, G. Cerullo, and C. Manzoni, Opt. Lett. **39**, 3849 (2014).
21. O. Dühr, E. T. J. Nibbering, G. Korn, G. Tempea, and F. Krausz, Opt. Lett. **24**, 34 (1999).
22. A. Fürbach, T. Le, C. Spielmann, and F. Krausz, Appl. Phys. B **70**, 37 (2000).
23. J. Liu, Y. Kida, T. Teramoto, and T. Kobayashi, Opt. Express **18**, 4664 (2010).
24. J. Liu, K. Okamura, Y. Kida, T. Teramoto, and T. Kobayashi, Opt. Express **18**, 20645 (2010).
25. A. Grün, D. R. Austin, S. L. Cousin, and J. Biegert, Opt. Lett. **40**, 4679 (2015).
26. M. Nisoli, S. De Silvestri, and O. Svelto, Appl. Phys. Lett. **68**, 2793 (1996).
27. A. Wirth, M. T. Hassan, I. Grguraš, J. Gagnon, A. Moulet, T. T. Luu, S. Pabst, R. Santra, Z. A. Alahmed, A. M. Azzeer, V. S. Yakovlev, V. Pervak, F. Krausz, and E. Goulielmakis, Science **334**, 195 (2011).
28. M. T. Hassan, A. Wirth, I. Grguraš, A. Moulet, T. T. Luu, J. Gagnon, V. Pervak, and E. Goulielmakis, Rev. Sci. Instrum. **83**, 111301 (2012).
29. M. T. Hassan, T. T. Luu, A. Moulet, O. Raskazovskaya, P. Zhokhov, M. Garg, N. Karpowicz, A. M. Zheltikov, V. Pervak, F. Krausz, and E. Goulielmakis, Nature **530**, 66 (2016).
30. R. Trebino, K. W. DeLong, D. N. Fittinghoff, J. N. Sweetser, M. A. Krumbügel, B. A. Richman, and D. J. Kane, Rev. Sci. Instrum. **68**, 3277 (1997).
31. R. Trebino, *Frequency-Resolved Optical Gating: The Measurement of Ultrashort Laser Pulses* (Springer, 2012).
32. F. Silva, M. Miranda, B. Alonso, J. Rauschenberger, V. Pervak, and H. Crespo, Opt. Express **22**, 10181 (2014).
33. Femtosoft Technologies, "FROG Ver. 3.2.4."